Journal of Petrology

Supplementary Materials for

Multi-stage metamorphism of the South Altyn ultrahigh-pressure metamorphic belt, West China: insights into tectonic evolution from continental subduction to back-arc extension

Jie Dong, Chunjing Wei

MOE Key Laboratory of Orogenic Belts and Crustal Evolution, School of Earth and Space Sciences, Peking University, Beijing 100871, China

Contents

Text S1: Analytical methods

Figure S1: $Mg+Fe^{2+}$ vs. Si (p.f.u. for O = 11) diagram showing the compositional variations of phengite inclusions in zircons for sample A1534 and A1533

Figure S2: Paragenesis diagrams for investigated samples A1533, A1534 and A1531

Figure S3: T-O/H_2O diagrams for samples A1533, A1534 and A1531

Figure S4: A binary diagram and profile of temperatures calculated based on Zr-in-Ttn thermometer for titanite from sample A1531

Table S1: Metamorphic ages of metamorphic rocks from the South Altyn Orogen

Table S2: Rock types and magmatic ages of early Paleozoic magmatite from the South Altyn domain

Table S3: ICP-OES whole-rock compositions (wt %) of garnet amphibolites and garnet-biotite gneisses from the South Altyn UHP belt

Table S4: Microprobe analyses of phengite for samples A1533 and A1534.

Table S5: Zr contents in titanite from sample A1531 and temperatures calculated based on the Zr-in-Titanite thermometer at 1.0 GPa.

Table S6: Zircon U-Pb isotopic and age data of garnet-biotite gneiss sample A1534

Table S7: Zircon U-Pb isotopic and age data of garnet amphibolite sample A1533

References

Text S1: Analytical methods

1. Bulk-rock composition analyses

The bulk-rock compositions were measured using a Leeman Prodigy inductively coupled plasma-optical emission spectroscopy (ICP-OES) system with high-dispersion Echelle optics at the China University of Geoscience (Beijing). The USGS (US Geological Survey) AGV-2 samples, and GSR-1, GSR-3, GSR-5 (National geological standard reference materials of China) were used as standards. The analytical precision (1σ) for most major elements is better than 1%, except for TiO_2 (~1.5%) and P_2O_5 (~2.0%). Loss on ignition was determined by placing 1 g of sample powder in a furnace at 1000 °C for several hours and reweighed in a desiccator (Song et al., 2018).

2. Mineral chemistry measurements

Mineral compositions were analyzed at Peking University using a JEOL JXA-8230 electron microprobe under the conditions with a 15 kV acceleration voltage, a 10 nA beam current, and a beam diameter of 1–2 μm for all analyses except biotite (5 μm). 53 kinds of natural and synthetic minerals from the SPI Company were used for standardization: sanidine was employed for K; rutile for Ti; chromium oxide for Cr; diopside for Ca and Mg; jadeite for Na, Al and Si; rhodonite for Mn and hematite for Fe. Representative mineral compositions are listed in Table 1 and Table 2.

3. Zircon U–Pb dating

Zircon grains from sample A1534 and A1533 were selected for LA-ICP-MS U–Pb dating and trace element measurements. They were separated by standard heavy liquid and magnetic separation followed by hand-picking under a binocular microscope. Zircon grains were mounted in two epoxy resins respectively, polished down to expose the zircon grain centers, photographed in transmitted and reflected light, and imaged using cathodoluminescence (CL).

U–Th–Pb isotopic ratios and trace element concentrations were measured at Peking University using an Agilent 7500c ICP-MS system connected with a 193 nm ArF Excimer laser system (COMPexPro 102) with automatic positioning system. The spot diameter is about 30 μm. Zircon 91500 and Plešovice were used as standards and the standard silicate glass NIST was used to calibrate the instrument. Elemental concentrations of U, Th and Pb were calibrated using ^{29}Si as an internal calibrant and NIST 610 as an external reference standard. $^{207}Pb/^{206}Pb$, $^{206}Pb/^{238}U$ and $^{207}Pb/^{235}U$ ratios and apparent ages were calculated using GLITTER 4.4 (Van Achterbergh et al., 2001).

In order to gain the ages of thin metamorphic zircon rims, a high spatial resolution (10 μm in diameter) LA-MC-ICP-MS U-Pb dating method using Nu Plasma II mass spectrometer coupled with GeoLas HD laser ablation system was applied at Peking University. Zircon references GJ-1 and Temora-2 were used as standards. The raw data was processed using software Iolite 3.71 (Paton et al., 2011) to gain the $^{238}U/^{206}Pb$, $^{206}Pb/^{238}U$ and $^{207}Pb/^{235}U$ ratios and apparent ages. U-Pb isotopic and age data are listed in Table S6 and Table S7. Age calculations and plots were processed using Isoplot (ver.4.15, Ludwig, 2012). The zircon standards of 91500, Plešovice, GJ-1, Temora-2 show concordia ages of 1063.5 ± 2.7 Ma (MSWD = 0.037, N = 18), 340.0 ± 0.94 Ma (MSWD = 0.20, N = 10), 601.2 ± 0.88 Ma (MSWD = 4.8, N = 28), 412.0 ±1.1 Ma (MSWD = 0.065, N = 10), which are in well accordance with the recommended values of 1062.4 ± 0.8 Ma (Wiedenbeck et al., 1995), 341.4 ± 1.3 Ma (Sláma et al., 2008), 602 ± 3 Ma (Gerdes and Zeh, 2006) and 416.78 ±0.33 Ma (Black et al., 2004) respectively.

4. Zr-in-titanite analysis

The Zr contents of titanite within thin sections from sample A1531 were measured using a ThermoFisher Scientific iCapRQ quadrupole-inductively coupled plasma-mass spectrometer coupled with a 193 nm GeoLas HD laser ablation system at Peking University. The spot size was fixed at 32 μm. NIST 610 was used as an external standard and ^{29}Si content measured from electron microprobe analyses was used as internal standard. Data reduction was carried out using

software Iolite 3.71 (Paton et al., 2011). The analytical precision is better than 5%. The Zr contents and Zr-in-titanite (Hayden et al., 2008) derived temperatures were presented in Table S5.

Figure S1

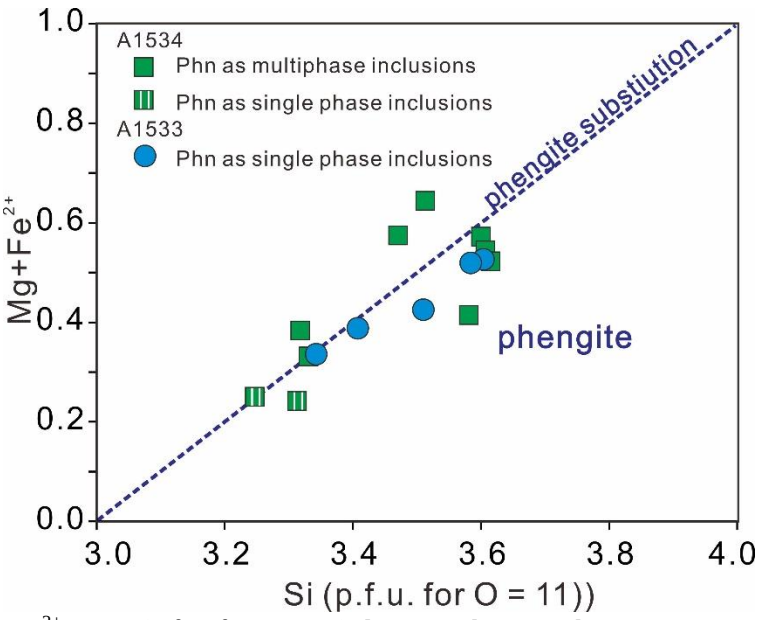

Figure. S1 $Mg+Fe^{2+}$ vs. Si (p.f.u. for O = 11) diagram showing the compositional variations of phengite inclusions in zircons.

Figure S2

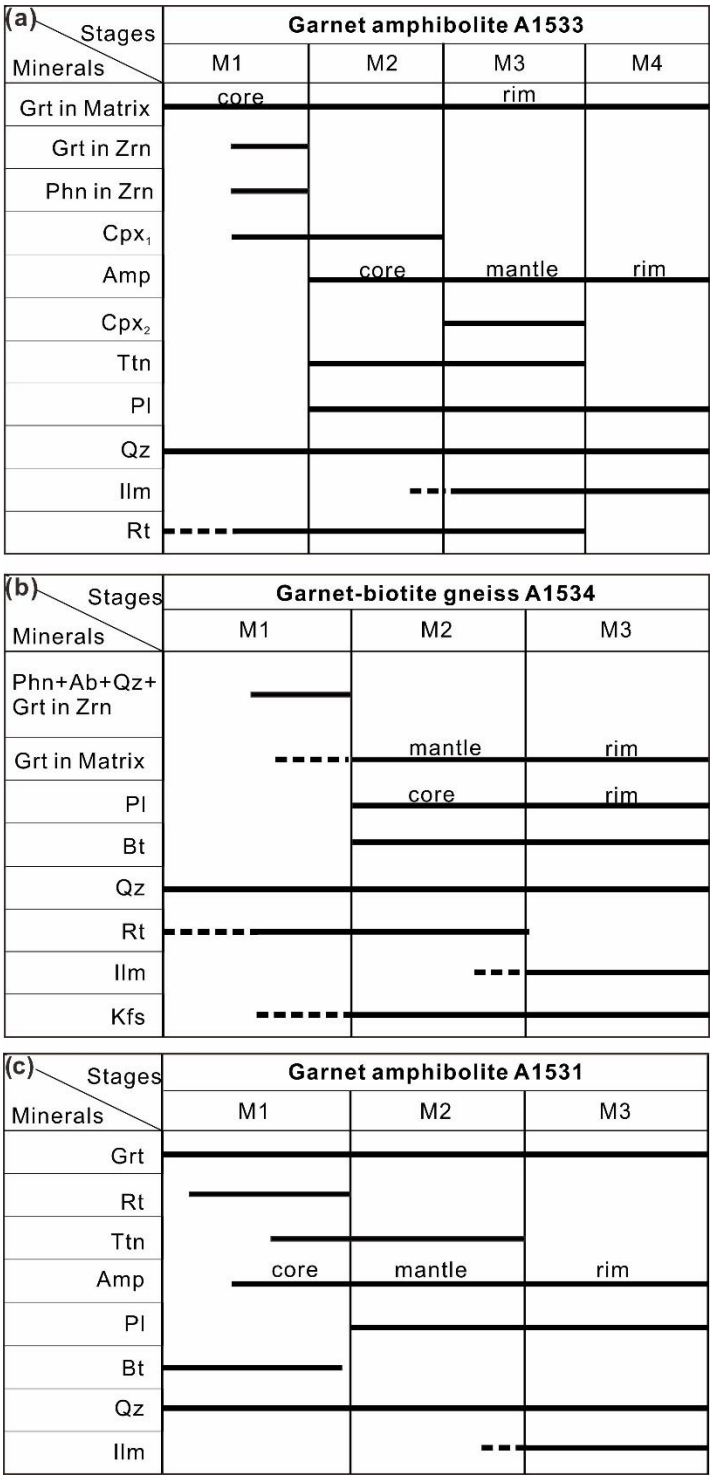

Figure S2. Paragenesis diagrams for investigated samples A1533 (a), A1534 (b) and A1531 (c).

Dashed lines refer to inferred presence of corresponding minerals.

Figure S3

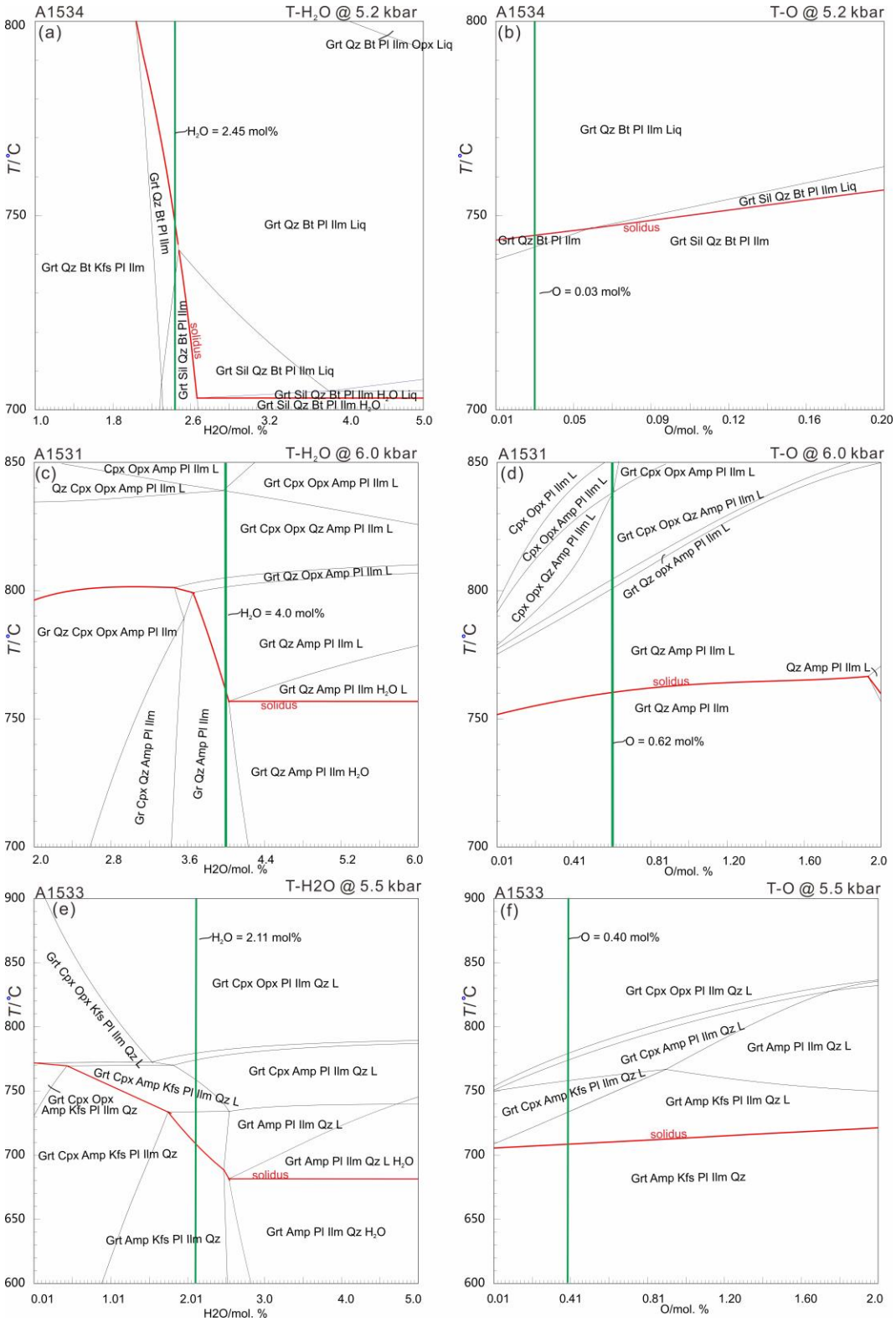

Figure S3. T-O/H_2O diagrams for samples A1534 (a, b), A1531 (c, d) and A1533 (e, f).

Figure S4

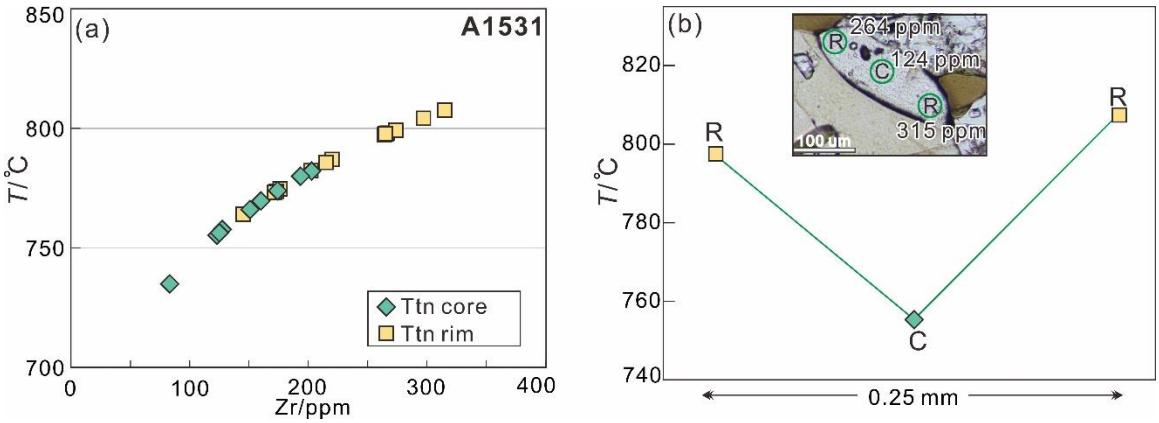

Figure. S4. A binary diagram and profile of temperatures calculated based on Zr-in-Ttn thermometer of Hydan et al. (2008) for titanite from sample A1531. C/R in (b) refers to the core and rim of titanite.

Table S1

Table S1. Metamorphic ages of metamorphic rocks from the South Altyn domain.

Localities	Rock types	Peak metamorphic ages（Ma）	Retrograde metamorphic ages（Ma）	Dating methods	References
Metamorphic rocks from South Altyn subduction-collision domain					
Jianggalesayi	Eclogite	493 ±4.3			Liu et al., 2007
	Garne-biotite paragneiss	499 ±27		LA-ICPMS	Liu et al., 2007
	Eclogite	500 ±2	455 ±2		Liu et al., 2012
	Eclogite	500 ±10		Sm–Nd	Zhang et al., 1999
	Eclogite	503.9 ±5.3		TIMS	Zhang et al., 1999
	Garnet-bearing biotite gneiss	503 ±5	456 ±4; 418 ±3		Cao et al., 2019a
	Kyanite-bearing garnet pelitic gneiss	484 ±3	450 ±2	LA-ICPMS	Cao et al., 2019b
	Eclogite	484 ±6			Zhang, 2006
	Granitic orthogneiss	454 ±4			Wang et al.,2013
Keqike Jianggalesayi	Coesite-bearing eclogite	501.3 ±2.1	462.9 ±2.4	LA-ICPMS	Gai et al., 2017; Gai, 2018
Tula	Sillimanite-bearing garnet paragneiss	447～462		TIMS	Zhang et al., 2000
	Garnet-bearing two-pyroxene granulite	450.2 ±4.1			Zhang et al., 2000
	Paragneiss	448 ±7		SHRIMP	Zhang et al., 2011
	Paragneiss	446 ±6		LA-ICPMS	Zhang et al., 2011
Younvsisayi	HP granitic granulite	497.8 ±2.7		LA-ICPMS	Ma et al., 2018
Yinggelisayi	Garnet-bearing granitic gneiss	487 ±10		SHRIMP	Zhang et al., 2004
	Garnet-bearing granitic gneiss	495 ±6.5			Zhang et al., 2004
	K-feldspar-bearing garnet pyroxenite	488.7 ±8.3		LA-ICPMS	Zhang, 2006; Liu et al., 2005
	Garnet-two pyroxene peridotite	509 ±12			Liu et al., 2009
	Garnet peridotite	498 ±3			Wang et al., 2011
	Garnet-bearing granitic gneiss	500 ±4		LA-ICPMS	Cao, 2013

Table S1continued

Localities	Rock types	Peak metamorphic ages（Ma）	Retrograde metamorphic ages（Ma）	Dating methods	References
Bashiwake	Garnet-bearing granitic gneiss	493 ±7		SHRIMP	Zhang et al., 2005
	Sapphirine-bearing mafic granulite	497 ±13			Zhang et al., 2005
	Garnet-two pyroxene peridotite	501 ±16		SHRIMP	Zhang et al., 2005
	Garnet peridotite	495.7 ±2.7			Li et al., 2013, 2015
	Garnet peridotite	503.3 ±3.1			Li et al., 2015
	Garnet pyroxenite	493 ±24		Sm–Nd	Li et al., 2015
	Felsic gneiss	508 ±11		LA-ICPMS	Wang et al., 2013
	Felsic granulite	495 ±4		SHRIMP	Zhang et al., 2014
	Felsic granulite	490 ±6.5	458 ±8.7		Zhang et al., 2014
	Felsic granulite	477 ±6	447 ±6	MC-LA-ICPMS rutile	Zhang et al., 2014
	Felsic granulite	480 ±5.5	448 ±5.7		Zhang et al., 2014
	Felsic granulite	486 ±7	435 ±13		Zhang et al., 2014
	Mafic granulite	497.2 ±4.5			Li et al., 2020
	Felsic granulite	500.1 ±2.7		LA-ICPMS	Dong et al., 2018
	Sapphirine-bearing mafic granulite	505.1 ±8.7			Dong et al., 2019
	Garnet-clinopyroxene mafic granulite	505.1 ±8.7			Dong et al., 2019
	Garnetite	500.0 ±5.4	486.1 ±5.2	SIMS	Dong et al., 2020
Danshuiquan	Garnet pyroxenite	475 ±4			Liu et al., 2009
	Garnet-bearing granitic gneiss	499 ±4			Liu et al., 2010
	HP granitic granulite	505 ±5			Zhu et al., 2014
	Kyanite-bearing garnet pelitic gneiss	486 ±5			Cao et al., 2009
	Felsic gneiss	500 ±5		LA-ICPMS	Wang et al., 2013
	Retrograde eclogite	502.1 ±4.7	484.1 ±1.6; 452.1 ±3.9		Gai, 2018
	Garnet-bearing granitic gneiss		488.2 ±2.1		Gai, 2018
	Garnet-bearing granitic gneiss		483.2 ±3.4		Gai, 2018

Table S1continued

Localities	Rock types	Peak metamorphic ages（Ma）	Retrograde metamorphic ages（Ma）	Dating methods	References
Danshuiquan	Garnet pyroxenite	505.2 ±3.8	485.6 ±2.2		Gai, 2018
	Garnet pyroxenite	500.1 ±3.5	485.5 ±5.9		Gai, 2018
	Kyanite-bearing garnet pelitic gneiss	501.2 ±1.7	484.1 ±1.4; 459.0 ±5.4		Gai, 2018
	Kyanite-bearing garnet pelitic gneiss	500.0 ±4.3	484.7 ±3.9	SIMS	Gai, 2018
	Mafic granulite	508 ±6		LA-ICPMS	Wang et al., 2016
Munabulake	Pelitic granulite	486 ±5		LA-ICPMS	Cao et al., 2013
	Two-muscovite felsdspar paragneiss	498 ±4			Cao et al., 2015
Piyazilekedaban	Garnet-amphibole-biotite orthogneiss	482 ±12		SHRIMP	Zhang et al., 2011
Kuoshi	Banded granitic gneiss	466 ±6		LA-ICPMS	Zhang et al., 2011
Qiemo	Granitic gneiss	505 ±3		LA-ICPMS	Zhang et al., 2011
Anatectic felsic veins/dykes from South Altyn subduction-collision domain					
Danshuiquan	Felsic vein in garnet pyroxenite		463.8 ±8.4	SIMS	Gai, 2018
	Felsic vein in garnet pyroxenite		469.6 ±6.9	SIMS	Gai, 2018
			460.5 ±5.4	LA-ICPMS	Gai, 2018

Table S2

Table S2. Rock types and magmatic ages of early Paleozoic magmatite from the South Altyn domain.

Localities	Rock serises	Age (Ma)	Dating methods	References
Magmatic rocks from South Altyn subduction-collision domain				
North of Gasi	Paleozoic Plutons	518 ±13	CAMECA	Cowgill et al., 2003
Changshagou	Plagioclase amphibolite-Pyroxene **peridotite**	510.6 ±1.4	LA-ICPMS	Guo et al., 2014
Changshagou	Granodiorite	503.1 ±1.7	LA-ICPMS	Kang, 2014
Yuemakeqi	Olivine pyroxenite-Pyroxene peridotite-amphibolite-**Gabbro**-Basalt (Ophiolite)	500.7 ±1.9	LA-ICPMS	Li et al., 2009
Yumuquan	**Granodiorite**-Monzogranite	496.9 ±1.9	LA-ICPMS	Sun et al., 2012
Mangya	Dunite-Harzburgite-Gabbro-**Basalt**	481.3 ±53	Sm-Nd	Liu et al., 1998
Ruoqiang Highway	Paleozoic Plutons	475 ±6	CAMECA	Cowgill et al., 2003
Mangya	Monzogranite	472.1 ±1.1	LA-ICPMS	Kang, 2014
South of Qingshuiquan	Pyroxenite	469.9 ±2.4		
North of Qingshuiquan	Peridotite-**Hornblende gabbro**-Quartz diorite-Granodiorite	467.4 ±1.4	LA-ICPMS	Ma et al., 2010, 2011
Changshagou	Gabbro	464.4 ±1.8		
North of Qingshuiquan	**Norite gabbro** (Layered mafic-ultramafic intrusions)	462.1 ±1.5		
Akalongtengshan	Quartz diorite	469 ±6	SHRIMP	Wu et al., 2014
Changshagou	Quartz diorite	469 ±3	LA-ICPMS	Wu et al., 2018
North of Mangya	Monzogranite	462 ±8	LA-ICPMS	Wu et al., 2018
Changshagou	Quartz diorite	467.5 ±2.4	LA-ICPMS	Dong et al., 2014
Changshagou	Quartz monzodiorite	468 ±2	LA-ICPMS	Dong et al., 2014
Changshagou	Gabbro	458.7 ±1.8	LA-ICPMS	Dong et al., 2014
Paxialayidang	Biotite monzogranite	465±2.9	LA-ICPMS	XACGS, 2003
North of Mangya	Diorite-**Quartz diorite**-Granodiorite-Monzogranite	465.6 ±4.6	SHRIMP	Wu et al., 2014
Tatelekebulake	Monzogranite	462 ±2	LA-ICPMS	Cao et al., 2010
Paxialayidang	**Muscovite monzogranite**-Syenogranite	460.1 ±3.9	LA-ICPMS	Zhang et al., 2016

Table S2 continued

Localities	Rock serises	Age (Ma)	Dating methods	References
Mangya	Quartz diorite	458.3 ±6.2	LA-ICPMS	Kang et al., 2016
West of Gasi	Paleozoic Plutons	457 ±6	CAMECA	Cowgill et al., 2003
Chaishuigou	Diabase	454 ±4	SHRIMP	Wu et al., 2014
Mangya	Diabase	453 ±5	LA-ICPMS	Wang et al., 2014
Dimunalike	Moyite	452.8 ±3.1	LA-ICPMS	Yang et al., 2012
Northwest of Mangya	Biotite granite	454.0 ±1.8	LA-ICPMS	Kang, 2014
Tula	Moyite	453.4 ±2.5	LA-ICPMS	Kang, 2014
Jianggalesayi	Monzogranite	453.1 ±2.1	LA-ICPMS	Kang, 2014
Ruoqiang river	Gneissic granite	451 ±1.7	LA-ICPMS	Kang, 2014
Qingshuiquan	Plagiogranite	451 ±4	LA-ICPMS	Wang et al., 2015
Kumudaban	Biotite monzogranite	449.7±5.8	LA-ICPMS	XACGS, 2003
Mangya	Hornblende gabbro	444.9±1.3	LA-ICPMS	Dong et al., 2011
Changshagou	Gabbro	444.9 ±3.4	SHRIMP	Xu et al., 2014
Yusupualeketage	Granite	448 ±1.0	TIMS	XACGS, 2003
Tatelekesu	Paleozoic Plutons	448 ±12	CAMECA	Cowgill et al., 2003
Yusupualeketage	Granodiorite	446 ±3	LA-ICPMS	Wang et al., 2014
Yusupualeketage	Monzogranite	431 ±9; 447 ±8	LA-ICPMS	Wang et al., 2014
West of Mangya	**Monzogranite**-Syenogranite	435 ±4	LA-ICPMS	Wu et al., 2018
Baiganhu	Granodiorite	444 ±5; 447 ±4; 448 ±2		
Yusupualeketage	Granite	440	LA-ICPMS	XACGS, 2003
Yusupualeketage	Moyite	424		Wang et al., 2008
Yusupualeketage	Aplitic dyke	421 ±3	LA-ICPMS	Wang et al., 2014
Changchungou	Monzogranite	411 ±5; 406 ±3	SHRIMP	Wu et al., 2014
Chaishuigou	**Monzogranite-Syenogranite**	406 ±4; 404 ±5		
Mangya	**Rhyolite-Dacite**-Basalt	406.1 ±1.2; 405.8±1.2	LA-ICPMS	Kang et al., 2015
Tula	Paleozoic Plutons	404 ±6	CAMECA	Cowgill et al., 2003
Chaishuigou	Monzogranite-**Syenogranite**-Alkali-feldspar granite	401 ±7	LA-ICPMS	Wu et al., 2018

Table S2 continued

Localities	Rock serises	Age (Ma)	Dating methods	References
Tula	Alkali-feldspar granite	385.2 ±8.1	SHRIMP	Wu et al., 2007
Anatectic felsic veins/dykes from South Altyn subduction-collision domain				
Jianggalesayi	Leucosome in garnet-bearing biotite gneiss	417 ±2	LA-ICPMS	Wang et al.,2013
Danshuiquan	Felsic vein in retrograde eclogite	486.7 ±1.2	LA-ICPMS	Gai, 2018
	Felsic vein in garnet pyroxenite	485.7 ±2.7	SIMS	Gai, 2018
		485.9 ±1.1	LA-ICPMS	Gai, 2018
	Felsic vein in garnet pyroxenite	488.4 ±3.7	SIMS	Gai, 2018
		484.2 ±3.1		Gai, 2018
	Felsic vein in garnet pyroxenite	486.3 ±2.9	LA-ICPMS	Gai, 2018
	Felsic vein in granitic gneiss	488.2 ±2.1		Gai, 2018
Yinggelisayi	Felsic vein in granitic gneiss	484.8 ±1.1	LA-ICPMS	Gai, 2018
	Monzogranitic dike in granitic gneiss	485.6 ±1.4		Gai, 2018

Notes: Bolded rocks from the rock series are dated

Table S3

Table S3. ICP-OES whole-rock compositions (wt %) of garnet amphibolite (A1531-33, A1535-36) and garnet-biotite gneiss (A1530, A1534) samples from Piyazilekedaban and Yaganbuyang areas, South Altyn UHP belt, West China.

	Samples	SiO_2	Al_2O_3	TFe_2O_3	CaO	MgO	K_2O	Na_2O	MnO	TiO_2	P_2O_5	LOI	Mg#
Yaganbuyang area	A1530	69.59	14.89	4.19	3.19	1.20	2.54	3.03	0.07	0.50	0.16	0.88	0.36
	A1531	47.63	13.44	17.60	9.43	5.97	0.56	0.52	0.25	3.45	0.31	0.40	0.40
	A1532	50.41	14.52	11.69	10.59	7.57	0.67	1.04	0.18	1.64	0.25	1.16	0.56
Piyazilekedaban area	A1533	56.11	12.59	17.17	8.03	2.19	0.80	0.24	0.26	2.19	0.49	0.28	0.20
	A1534	61.21	17.42	7.71	3.85	2.50	2.34	3.42	0.07	0.68	0.17	0.73	0.39
	A1535	58.22	13.18	16.24	5.85	2.24	0.83	0.22	0.23	2.19	0.41	0.05	0.21
	A1536	53.69	13.42	15.92	7.43	3.96	1.43	0.59	0.21	2.04	0.26	1.02	0.33

Table S4

Table S4. Microprobe analyses of phengite for samples A1533 and A1534.

	A1534										A1533				
	S	S	M	M	M	M	M	M	M	M	S	S	S	S	S
SiO_2	48.97	50.26	49.49	49.90	52.47	54.22	50.47	53.67	50.91	51.21	51.78	51.30	55.45	51.17	50.32
TiO_2	0.07	0.08	0.06	0.05	0.24	0.20	0.22	0.18	-	-	0.79	1.01	0.19	0.28	1.32
Al_2O_3	30.76	30.29	29.61	28.51	22.97	24.72	19.14	23.25	24.43	23.12	25.87	28.10	24.76	23.23	27.59
Cr_2O_3	0.04	0.02	-	-	-	-	-	0.01	-	-	0.01	-	0.06	0.02	-
FeO	3.99	4.06	4.06	3.79	5.88	5.64	8.54	6.26	3.32	3.10	3.50	2.83	3.89	3.26	3.86
MnO	-	0.04	-	0.02	0.04	-	0.14	0.03	-	-	0.04	-	-	-	-
MgO	1.86	1.55	1.55	2.69	2.30	2.25	2.82	2.24	5.09	5.78	2.25	2.33	3.35	3.14	2.75
CaO	-	0.05	-	0.05	0.17	0.12	0.65	0.35	0.33	0.41	0.07	0.05	0.06	0.02	0.12
Na_2O	0.21	0.29	0.34	0.23	0.37	0.29	0.24	0.39	0.14	0.17	0.18	0.30	0.15	0.14	0.24
K_2O	9.24	8.72	10.32	9.25	8.61	7.35	7.15	7.54	7.01	6.77	8.12	8.78	8.86	8.83	8.38
Sum	95.14	95.36	95.43	94.49	93.05	94.79	89.37	93.92	91.23	90.56	92.61	94.70	96.77	90.09	94.58
O	11	11	11	11	11	11	11	11	11	11	11	11	11	11	11
Si	3.25	3.31	3.32	3.33	3.60	3.58	3.61	3.62	3.47	3.51	3.51	3.41	3.60	3.58	3.34
Ti	0.00	0.00	0.00	0.00	0.01	0.01	0.01	0.01	0.00	0.00	0.04	0.05	0.01	0.02	0.07
Al	2.41	2.35	2.34	2.24	1.86	1.93	1.61	1.85	1.96	1.87	2.07	2.20	1.90	1.92	2.16
Cr	0.00	0.00	0.00	0.00	0.00	0.00	0.00	0.00	0.00	0.00	0.00	0.00	0.00	0.00	0.00
Fe^{3+}	0.16	0.13	0.00	0.15	0.00	0.12	0.27	0.06	0.13	0.12	0.00	0.00	0.01	0.00	0.15
Fe^{2+}	0.07	0.09	0.23	0.06	0.34	0.19	0.24	0.30	0.06	0.05	0.20	0.16	0.20	0.19	0.06
Mn	0.00	0.00	0.00	0.00	0.00	0.00	0.01	0.00	0.00	0.00	0.00	0.00	0.00	0.00	0.00
Mg	0.18	0.15	0.16	0.27	0.24	0.22	0.30	0.23	0.52	0.59	0.23	0.23	0.33	0.33	0.27
Ca	0.00	0.00	0.00	0.00	0.01	0.01	0.05	0.03	0.02	0.03	0.01	0.00	0.00	0.00	0.01
Na	0.03	0.04	0.04	0.03	0.05	0.04	0.03	0.05	0.02	0.02	0.02	0.04	0.02	0.02	0.03
K	0.78	0.73	0.88	0.79	0.75	0.62	0.65	0.65	0.61	0.59	0.70	0.74	0.74	0.79	0.71
Sum	6.87	6.82	6.97	6.88	6.86	6.72	6.79	6.78	6.80	6.80	6.78	6.83	6.81	6.85	6.81
Si-3	0.25	0.31	0.32	0.33	0.60	0.58	0.61	0.62	0.47	0.51	0.51	0.41	0.60	0.58	0.34
Fe+Mg	0.25	0.24	0.38	0.33	0.57	0.41	0.54	0.52	0.57	0.64	0.43	0.40	0.53	0.52	0.34
Si*	3.25	3.24	3.32	3.33	3.57	3.41	3.54	3.52	3.47	3.51	3.43	3.40	3.53	3.52	0.34

Notes: S/M stands for **s**ingle phase inclusions or **m**ultiphase inclusions. Si* (normalized Si contents) equals to Fe+Mg when Si-3 > Fe+Mg and equals to Si if Si-3 < Fe+Mg.

Table S5

Table S5. Zr contents in titanite from sample A1531 and temperatures calculated based on the Zr-in-Titanite thermometer at 1.0 GPa.

Spots	Zr/ppm	2δ	T/ ℃	2δ	Notes
A1531-1	215.2	6.9	786	2	R
A1531-2	150.8	7.0	766	2	C
A1531-3	83.2	5.2	735	3	C
A1531-4	145.0	5.9	764	2	R
A1531-5	126.5	6.4	757	3	C
A1531-6	176.2	6.1	775	2	R
A1531-7	219.9	8.7	787	2	R
A1531-8	160.1	9.4	769	3	C
A1531-9	215.2	6.9	786	2	R
A1531-10	266.7	9.7	798	2	R
A1531-11	266.0	10.0	798	2	R
A1531-12	203.0	5.9	782	2	C
A1531-13	265.7	8.9	798	2	R
A1531-14	297.0	14.0	804	3	R
A1531-15	173.0	20.0	774	6	R
A1531-16	127.8	9.8	757	4	C
A1531-17	171.5	5.5	773	2	R
A1531-18	264.0	11.0	797	2	R
A1531-19	194.0	11.0	780	3	C
A1531-20	123.7	5.9	756	2	C
A1531-21	273.0	11.0	799	2	R
A1531-22	315.0	11.0	808	2	R
A1531-23	174.0	11.0	774	3	C
A1531-24	202.2	8.5	782	2	R

Notes: C/R refers to the core and rim of titanite where the analyses locate.

Table S6

Table S6: Zircon U-Pb isotopic and age data of garnet-biotite gneiss sample A1534.

Spots	Isotope ratios				Corrected ages(Ma)					
	$^{207}Pb/^{235}U$	1δ	$^{206}Pb/^{238}U$	1δ	$^{207}Pb/^{206}Pb$	1δ	$^{207}Pb/^{235}U$	1δ	$^{206}Pb/^{238}U$	1δ
LA-ICP-MS method with spot diameter of 30 μm										
A1534-01	0.638	0.010	0.081	0.001	485	21	501	6	504	4
A1534-02	0.637	0.009	0.081	0.001	488	17	500	5	503	4
A1534-03	0.641	0.014	0.081	0.001	518	31	503	9	500	5
A1534-04	0.596	0.010	0.077	0.001	458	23	475	6	478	4
A1534-05	0.649	0.013	0.082	0.001	508	27	508	8	508	5
A1534-06	0.602	0.009	0.078	0.001	463	19	479	6	482	4
A1534-07	0.650	0.010	0.081	0.001	531	20	508	6	503	4
A1534-08	0.604	0.011	0.075	0.001	553	23	480	7	464	4
A1534-09	0.623	0.012	0.081	0.001	448	27	491	7	500	4
A1534-10	0.648	0.010	0.081	0.001	533	20	507	6	501	4
A1534-11	0.613	0.011	0.078	0.001	483	25	485	7	486	4
A1534-12	0.655	0.013	0.082	0.001	535	28	511	8	506	5
A1534-13	0.619	0.011	0.080	0.001	448	24	489	7	498	4
A1534-14	0.761	0.013	0.087	0.001	650	42	558	7	536	4
A1534-15	0.613	0.010	0.078	0.001	484	21	486	6	486	4
A1534-16	0.627	0.011	0.082	0.001	436	25	494	7	507	4
A1534-17	0.595	0.012	0.077	0.001	442	27	474	7	481	4
A1534-18	0.966	0.017	0.105	0.001	763	44	671	9	644	5
A1534-19	0.626	0.012	0.080	0.001	467	26	493	7	499	4
A1534-20	1.185	0.018	0.119	0.001	928	36	777	8	725	6
A1534-21	0.644	0.011	0.081	0.001	511	23	505	7	504	4
A1534-22	0.869	0.017	0.104	0.001	628	26	635	9	637	6
A1534-23	0.609	0.011	0.077	0.001	513	25	483	7	476	4
A1534-24	0.758	0.015	0.090	0.001	571	48	559	8	556	5
A1534-25	0.624	0.010	0.080	0.001	486	21	492	6	494	4
A1534-26	0.621	0.010	0.080	0.001	456	21	490	6	498	4
A1534-27	0.633	0.013	0.074	0.001	501	57	466	9	459	4
A1534-28	0.606	0.012	0.078	0.001	478	27	481	8	482	4
LA-MC-ICP-MS method with spot diameter of 10 μm										
A1534-29	0.622	0.011	0.078	0.001	468	31.5	488	7	484	4.5
A1534-30	0.595	0.009	0.076	0.001	460	22.5	472	5.5	469	4.5
A1534-31	0.642	0.008	0.077	0.001	581	24	502	5	481	3.5
A1534-32	0.587	0.010	0.074	0.001	493	28	469	6	460	5
A1534-33	0.613	0.007	0.078	0.001	489	15	484	4.5	482	4.5
A1534-34	0.647	0.010	0.080	0.001	509	27.5	504	6	498	5
A1534-35	0.591	0.008	0.075	0.001	482	24.5	469	5	467	4
A1534-36	0.597	0.011	0.078	0.001	388	33.5	473	6.5	486	5.5

Table S6 continued

Spots	Isotope ratios				Corrected ages(Ma)					
	$^{207}Pb/^{235}U$	1δ	$^{206}Pb/^{238}U$	1δ	$^{207}Pb/^{206}Pb$	1δ	$^{207}Pb/^{235}U$	1δ	$^{206}Pb/^{238}U$	1δ
LA-MC-ICP-MS method with spot diameter of 10 μm										
A1534-37	0.587	0.008	0.077	0.001	440	23	467	5	475	5
A1534-38	0.620	0.010	0.080	0.001	449	27	489	6	494	5.5
A1534-39	0.612	0.010	0.078	0.001	484	32	482	6.5	485	5
A1534-40	0.622	0.008	0.080	0.001	482	14.5	489	5	494	6
A1534-41	0.621	0.007	0.081	0.001	463	17	489	4.5	499	4.5
A1534-42	0.614	0.008	0.077	0.001	522	21	485	5	479	4
A1534-43	0.617	0.008	0.079	0.001	494	18	487	5	488	4.5
A1534-44	0.617	0.010	0.080	0.001	435	24	486	6	498	5
A1534-45	0.611	0.007	0.078	0.001	500	16	483	4.5	483	4
A1534-46	0.650	0.010	0.083	0.001	506	26.5	506	6	512	5.5

1δ refers to 1 sigma of standard deviation.

Table S7

Table S7: Zircon U-Pb isotopic and age data of garnet amphibolite sample A1533.

Spots	Isotope ratios				Corrected ages(Ma)					
	$^{207}Pb/^{235}U$	1δ	$^{206}Pb/^{238}U$	1δ	$^{207}Pb/^{206}Pb$	1δ	$^{207}Pb/^{235}U$	1δ	$^{206}Pb/^{238}U$	1δ
LA-ICP-MS method with spot diameter of 30 μm										
A1533-01	0.612	0.009	0.077	0.001	517	18	485	6	478	4
A1533-02	0.613	0.009	0.077	0.001	510	19	486	6	480	4
A1533-03	1.017	0.012	0.107	0.001	891	13	712	6	657	5
A1533-04	0.607	0.008	0.078	0.001	476	15	482	5	483	4
A1533-05	1.107	0.013	0.121	0.001	812	12	757	6	738	5
A1533-06	0.611	0.008	0.077	0.001	510	17	484	5	478	4
A1533-07	0.604	0.008	0.076	0.001	493	35	477	5	474	4
A1533-08	0.561	0.008	0.072	0.001	486	18	452	5	446	4
A1533-09	0.598	0.008	0.077	0.001	474	16	476	5	476	4
A1533-10	1.085	0.012	0.119	0.001	812	12	746	6	724	5
A1533-11	1.079	0.014	0.114	0.001	756	35	708	7	693	5
A1533-12	0.613	0.009	0.077	0.001	497	36	482	5	478	4
A1533-13	1.436	0.016	0.152	0.001	889	12	904	7	910	6
A1533-14	0.610	0.009	0.078	0.001	476	19	484	6	485	4
A1533-15	0.611	0.008	0.078	0.001	479	16	484	5	485	4
A1533-16	0.635	0.010	0.081	0.001	488	20	499	6	501	4
A1533-17	0.647	0.009	0.081	0.001	515	18	506	6	504	4
A1533-18	0.609	0.008	0.078	0.001	479	17	483	5	484	4
A1533-19	0.623	0.008	0.080	0.001	458	16	492	5	499	4
A1533-20	0.633	0.009	0.082	0.001	461	17	498	5	506	4
A1533-21	0.613	0.013	0.078	0.001	485	29	485	8	485	4
A1533-22	0.615	0.009	0.079	0.001	476	19	487	6	489	4
A1533-23	0.614	0.009	0.078	0.001	486	18	486	6	486	4
LA-MC-ICP-MS method with spot diameter of 10 μm										
A1533-24	0.622	0.007	0.078	0.001	504	15	490	5	486	5
A1533-25	0.590	0.009	0.075	0.001	461	29	470	6	465	4
A1533-26	0.602	0.020	0.075	0.001	440	50	465	11	465	9
A1533-27	0.606	0.006	0.078	0.001	451	15	480	4	484	4
A1533-28	0.615	0.007	0.079	0.001	479	12	486	5	488	5
A1533-29	0.605	0.007	0.077	0.001	491	15	479	4	479	5
A1533-30	0.584	0.007	0.076	0.001	453	14	466	4	469	4
A1533-31	0.610	0.007	0.078	0.001	482	13	482	4	485	5
A1533-32	0.636	0.007	0.082	0.001	483	10	499	4	507	4
A1533-33	0.604	0.006	0.077	0.001	492	15	479	4	481	4
A1533-34	0.621	0.009	0.079	0.001	492	22	489	6	489	5
A1533-35	0.605	0.006	0.077	0.001	482	15	480	4	480	4
A1533-36	0.612	0.006	0.078	0.001	491	11	484	4	481	4
A1533-37	0.638	0.007	0.081	0.001	501	14	501	4	499	4

Table S7 continued

Spots	Isotope ratios				Corrected ages(Ma)					
	$^{207}Pb/^{235}U$	1δ	$^{206}Pb/^{238}U$	1δ	$^{207}Pb/^{206}Pb$	1δ	$^{207}Pb/^{235}U$	1δ	$^{206}Pb/^{238}U$	1δ
A1533-38	0.609	0.007	0.077	0.001	479	14	482	4	478	4
A1533-39	0.619	0.006	0.079	0.001	470	13	488	4	490	4
A1533-40	0.625	0.006	0.079	0.001	491	11	493	4	488	4
A1533-41	0.608	0.006	0.076	0.001	498	13	482	4	472	4

1δ refers to 1 sigma of standard deviation.

References

Black, L. P., Kamo, S. L., Allen, C. M., Davis, D. W., Aleinikoff, J. N., Valley, J. W., ... & Foudoulis, C. (2004). Improved 206Pb/238U microprobe geochronology by the monitoring of a trace-element-related matrix effect; SHRIMP, ID–TIMS, ELA–ICP–MS and oxygen isotope documentation for a series of zircon standards. *Chemical Geology* **205**(1-2), 115-140.

Cao, Y. T. (2013). Metamorphic evolution and fluid-melt behavior of HP-UHP rocks from South Altyn and Shenglikou area of North Qaidam UHP belt. Northwest University, Doctoral dissertation (in Chinese with English abstract).

Cao, Y. T., Liu, L., Wang, C., Yang, W. Q. & Zhu, X. H. (2010). Geochemical, zircon U-Pb dating and Hf isotope compositions studies for Tatelekebulake granite in south Altyn Tagh. *Acta Petrologica Sinica* **26**, 3259-3271.

Cao, Y. T., Liu, L., Wang, C., et al. (2015). LA-ICP-MS Zircon U-Pb Dating of Bashikourgan Rock Group of Changcheng System in Munabulake Area of Southern Altun Mountains and Its Significance. *Geological Bulletin of China* **34**, 1446–1458 (in Chinese with English Abstract).

Cao, Y. T., Liu, L., Wang, C., Chen, D. L. & Zhang, A. D. (2009). P–T path of Early Paleozoic pelitic high-pressure granulite from Danshuiquan area in Altyn Tagh. Acta Petrologica Sinica 25, 2260–2270 (in Chinese with English abstract).

Cao, Y. T., Liu, L., Wang, C., Kang, L., Yang, W., Liang, S., Liao, X. & Wang, Y. (2013). Determination and Implication of the HP Pelitic Granulite from the Munabulake Area in the South Altyn Tagh. *Acta Petrologica Sinica* **29**, 1727–1739 (in Chinese with English Abstract)

Cao, Y. T., Liu, L., Wang, C., Kang, L., Li, D., Yang, W. Q., & Zhu, X. H. (2019a). Timing and nature of the partial melting processes during the exhumation of the garnet–bearing biotite gneiss in the southern Altyn Tagh HP/UHP belt, Western China. *Journal of Asian Earth Sciences* **170**, 274-293.

Cao, Y., Liu, L., Wang, C., Zhang, C., Kang, L., Yang, W. & Zhu, X. (2019b). Multi-Stage Metamorphism of the UHP Pelitic Gneiss from the Southern Altyn Tagh HP/UHP Belt, Western China: Petrological and Geochronological Evidence. *Journal of Earth Science* **30**, 603-620.

Cowgill, E., Yin, A., Harrison, T. M. & Wang, X. F. (2003). Reconstruction of the Altyn Tagh fault based on U–Pb ion microprobe geochronology: role of back thrusts, mantle sutures, and heterogeneous crustal strength in forming the Tibetan Plateau. *Journal of Geophysical Research* **108**, 2346.

Dong, H. K. , Guo, J. C., Chen, H. Y., Ti, Z. H., Liu, G. & Liu, S. L., Xue, P. Y. & Xing, P. (2014). Evolution characteristics of Ordovician intrusive rock in Changshagou of Altun region. *Northwestern Geology* **47**, 73-87.

Dong, J., Wei, C. J., Clarke, G. L. & Zhang, J. X. (2018). Metamorphic evolution during deep subduction and exhumation of continental crust: insights from felsic granulites in South Altyn Tagh, West China. *Journal of Petrology 59*(10), 1965–1990.

Dong, J., Wei, C. & Zhang, J. (2019). Ultra high temperature metamorphism of mafic granulites from South Altyn Orogen, West China: A result from the rapid exhumation of deeply subducted continental crust. *Journal of Metamorphic Geology 37*(3), 315–338.

Dong, J., Wei, C., Chen, J. & Zhang, J. (2020). P–T–t path of garnetites in South Altyn Tagh, West China: a complete record of the ultradeep subduction and exhumation of continental crust. *Journal of Geophysical Research: Solid Earth* **125**, e2019JB018881.

Dong, Z. C., Xiao, P. X., Xi, R. G., Guo, L. & Gao, X. F. (2011). Geochemical characteristics and isotopic dating of bojites in the tectonic melange belt on south margin of Altun. *Geological Review* **57**(2), 207-216.

Gai, Y., Liu, L., Wang, C., Yang, W., Kang, L., Cao, Y. & Liao, X. (2017). Discovery of coesite in eclogite from Keqike Jianggalesayi: new evidence for ultrahigh-pressure metamorphism in South Altyn Tagh, northwestern China. *Science Bulletin* **62**(15), 1048–1051.

Gai, Y. S. (2018). Differential exhumation and partial melting of HP-UHP metamorphic rocks in South Altyn Tagh, NW China. Northwest University, Doctoral dissertation (in Chinese with English abstract).

Gerdes, A., & Zeh, A. (2006). Combined U–Pb and Hf isotope LA-(MC-) ICP-MS analyses of detrital zircons: comparison with SHRIMP and new constraints for the provenance and age of an Armorican metasediment in Central Germany. *Earth and Planetary Science Letters* **249**(1-2), 47-61.

Guo, J. C., Xu, X. M., Chen, H. Y., Li, X., Dong, H. K. & Ti, Z. H. (2014). Zircon U–Pb age and geological implications of ultramafic rocks in Changshagou, Altun area, Xingjiang Province. *Northwestern Geology* **47**(4), 170–177 (in Chinese with English abstract).

Hayden, L. A., Watson, E. B., & Wark, D. A. (2008). A thermobarometer for sphene (titanite). *Contributions to Mineralogy and Petrology* **155**(4), 529-540.

Kang, L. (2014). Early Paleozoic Multi-stage granitic magmatism and the geological significance in the South Altyn Tagh HP-UHP metamorphic belt. Northwest University, Doctoral dissertation (in Chinese with English abstract).

Kang, L., Xiao, P. X., Gao, X. F., Xi, R. G. & Yang, Z. C. (2016). Chronology, geochemistry and petrogenesis of monzonitic granite and quartz diorite in Mangai area: Its inspiration to Early Paleozoic tectonic - magmatic evolution of the southern Altyn Tagh. *Acta Petrologica Sinica* **32**(6), 1731-1748.

Kang, L., Xiao, P. X., Gao, X. F., Xi, R. G. & Yang, Z. C. (2015). Age, petrogenesis and tectonic implications of Early Devonian bimodal volcanic rocks in the South Altyn, NW China. *Journal of Asian Earth Sciences* **111**, 733-750.

Li, X. M. , Ma, Z. P. , Sun, J. M. , Xu, X. Y. & Duan, X. X. (2009). Characteristics and age study about the yuemakeqi mafic-ultramagic rock in the southern altyn fault. *Acta Petrologica Sinica* **25**(4), 862-872.

Li, Y., Zhang, J., Yu, S., Li, S. & Gong, J. (2015). Origin of Early Paleozoic garnet peridotite and associated garnet pyroxenite in the south Altyn Tagh, NW China: constraints from geochemistry, SHRIMP U–Pb zircon dating and Hf isotopes. *Journal of Asian Earth Sciences* **100**, 60-77.

Li, Y. S., Zhang, J. X., Li, S. R., Yu, S. Y., Gong, J. H., Lin, Y. H. (2013). Metamorphic evolution of the Bashiwake garnet peridotite from the South Altyn Tagh. Acta Petrol. Sinica 29 (6), 2073–2092 (in Chinese with English abstract).

Li, Y., Zhang, J., Li, Y., Mostofa, K. M., Yu, S., Guo, J., ... & Zhou, G. (2020). Petrogenesis of mafic granulite in South Altyn Tagh, NW China: Constraints from petrology, zircon U–Pb chronology, and geochemistry. *Geological Journal* **55**(2), 1431-1449.

Liu, L., Che, Z. C., Wang, Y., Luo, J. H., Wang, J. Q. & Gao, Z. J. (1998). The evidence of Sm-Nd isochron age for the early paleozoic ophiolite in Mangya area, Altun Mountains. *Chinese Science Bulletin* **43**, 754–756.

Liu, L., Chen, D. L., Zhang, A. D., Sun, Y., Wang, Y., Yang, J. X. & Luo, J. H. (2005). Ultrahigh pressure gneissic K-feldspar garnet clinopyroxenite in the Altyn Tagh, NW China evidence from clinopyroxene exsolution in garnet. *Science in China* **48**, 1000–1010.

Lin, L., Zhang, A., Chen, D., Yang, J., Luo, J. & Wang, C. (2007). Implications based on LA-ICP-Ms zircon U-Pb ages of eclogite and its conntry rock from Jianggalesayi area, Altyn tagh. *Earth Science Frontiers* **14**(1):098-107.

Liu, L., Wang, C., Chen, D.L., Zhang, A.D. & Liou, J.G. (2009). Petrology and geochronology of HP-UHP rocks from the South Altyn, northwestern China. *Journal of Asian Earth Sciences* **35**, 232–244.

Liu, L., Yang, J.X., Chen, D.L., Wang, C., Zhang, C.L., Yang, W.Q. & Cao, Y.T. (2010). Progress and controversy in the study of HP-UHP metamorphic terranes in the West and Middle Central China orogen. *Journal of Earth Science* **21**, 581–597.

Liu, L., Wang, C., Cao, Y. T., Chen, D. L., Kang, L., Yang, W. Q. & Zhu, X. H. (2012). Geochronology of multi-stage metamorphic events: constraints on episodic zircon growth from the UHP eclogite in the South Altyn, NW China. *Lithos* **136–139**, 10–26.

Ludwig, K.R. (2012). Isoplot v. 3.75: A Geochronological Toolkit for Microsoft Excel: Berkeley Geochronology Center Special Publication 5, 75 p.

Ma, T., Liu, L., Gai, Y. S., Wang, C., Kang, L., Liao, X.Y., Pak, S. W. & Zhang, K. (2018). Discovery of the high pressure granitic granulite in South Altyn and it's geological significance. *Acta Petrologica Sinica* **34**(12), 3643–3657 (in Chinese with English abstract).

Ma, Z. P., Li, X. M., Xu, X. Y., Sun, J. M., Tang, Z. & Du, T. (2011). Zircon LA-ICP-MS U-Pb isotopic dating for Qingshuiquan layered mafic-ultramafic intrusion southern Altun orogeny in northwestern China and its implication. *Geology in China* **38**(4), 1071-1078 (in Chinese with English abstract).

Ma, Z. P., Sun, J. M., Zhuo, T., Li, X. M., Xu, X. Y., Lei, Y. X., Wang, L. & Duan, X. (2010). Discussions on the magmatic Cu-Ni-PGE sulfides mineralization potential of the Changshagou-Qingshuiquan layered mafic-ultramafic intrusions, Altyn Tagh. *Northwestern Geology* **43**(4), 18-24 (in Chinese with English abstract).

Paton, C., Hellstrom, J., Paul, B., Woodhead, J. & Hergt, J. (2011). Iolite: Freeware for the visualisation and processing of mass spectrometric data. *Journal of Analytical Atomic Spectrometry* **26**, 2508-2518.

Sláma, J., Košler, J., Condon, D. J., Crowley, J. L., Gerdes, A., Hanchar, J. M., ... & Whitehouse, M. J. (2008). Plešovice zircon—a new natural reference material for U–Pb and Hf isotopic microanalysis. *Chemical Geology* **249**(1-2), 1-35.

Song, S., Bi, H., Qi, S., Yang, L., Allen, M. B., Niu, Y., Su, L. & Li, W. (2018). HP–UHP Metamorphic Belt in the East Kunlun Orogen: Final Closure of the Proto-Tethys Ocean and Formation of the Pan-North-China Continent. *Journal of Petrology* **59**(11), 2043–2060.

Sun, J. M., Ma, Z. P., Tang, Z. & Li, X. M. (2012). The LA-ICP-MS zircon dating and tectonic significance of the Yumuquan magmamixing granite, southern Altyn Tagh. *Acta Geologica Sinica* **86**, 247–257 (in Chinese with English abstract).

Van Achterbergh, E., Ryan, C., Jackson, S. & Griffin, W. L. (2001). Data reduction software for LA-ICP-MS. In: Laser-Ablation-ICPMS in the Earth Sciences: Principles and Applications, vol. 29 (ed Sylvester, P.) Mineralogical Society of Canada, Ottawa, Canada, pp. 239–243.

Wang, C., Liu, L., Yang, W. Q., Zhu, X. H., Cao, Y. T., Kang, L., Shen, S. F., Li, R. & He, S. (2013). Provenance and ages of the Altyn complex in Altyn Tagh: implications for the early Neoproterozoic evolution of northwestern China. *Precambrian Research* **230**, 193–208.

Wang, C., Liu, L., Xiao, P. X., Cao, Y. T., Yu, H. Y., Meert, J. G. & Liang, W. T. (2014). Geochemical and geochronologic constraints for Paleozoic magmatism related to the orogenic collapse in the Qimantagh–South Altyn region, northwestern China. *Lithos* **202**, 1-20.

Wang, C., Liu, L., Chen, D. L. & Cao, Y. T. (2011). Petrology, geochemistry, geochronology and metamorphic evolution of garnet peridotites from South Altyn Tagh UHP terrane, NW China: records related to crustal slab subduction and exhumation history. In: Dobrzhinetskaya, L., Faryad, W., Wallis, S., Cuthbert, S. (Eds.) Ultrahigh Pressure Metamorphism: 25 Years after the Discovery of Metamorphic Coesite and Diamond. Elsevier, London, pp. 541–576.

Wang, L., Yang, P., Duan, X., Long, X. & Sun, J. (2016). Isotopic age and genesis of plagiogranite from Qingshuiquan area in the middle of South Altyn Tagh. *Acta Petrologica Sinica* **32**(3), 759-774.

Wang, L., Li, Z., Yang, P., Liu, Y., Zhou, N. & Wei, X. (2016). New Evidences for the Closure of the Altyn Proto-Tethys Ocean: A Case Study of High Pressure Basic Granulites from Ring Hills in the Altyn Mountains. *Bulletin of Mineralogy, Petrology and Geochemistry* **35**(5), 897-907.

Wiedenbeck, M. A. P. C., Alle, P., Corfu, F., Griffin, W. L., Meier, M., Oberli, F. V., ... & Spiegel, W. (1995). Three natural zircon standards for U-Th-Pb, Lu-Hf, trace element and REE analyses. *Geostandards newsletter* **19**(1), 1-23.

Wu, C., Chen, H., Wu, D. & Ernst, W. G. (2018). Paleozoic granitic magmatism and tectonic evolution of the South Altun block, NW China: Constraints from zircon U-Pb dating and Lu-Hf isotope geochemistry. *Journal of Asian Earth Sciences* **160**, 168-199.

Wu, C., Gao, Y., Lei, M., Qin, H., Liu, C., Li, Z. & Wooden, J. L. (2014). Zircon SHRIMP U-Pb dating, Lu-Hf isotopic characteristics and petrogenesis of the Palaeozoic granites in Mangya area, southern Altun, NW China. *Acta Petrologica Sinica* **30**(8), 2297-2323.

Wu, S. P., Wu, C. L. & Chen, Q. L. (2007). Characteristics and tectonic setting of the Tula aluminous A-type granite at the south side of the Altyn Tagh fault, NW China. *Geological Bulletin of China* **26**(10), 1385-1392.

XACGS. (2003). Geological Map of the Suwushijie, Xinjiang China, Scale 1: 250, 000. Xi'an Center of Geological Survey, China Geological Survey, Xi'an (in Chinese).

Xu, X., Guo, J., Chen, H., Duan, X., Zhang, Z. & Zhang, Z. (2014). SHRIMP zircon U-Pb age and geochemical characteristics of ordovician gabbro from Altun, Xinjiang province. *Northwestern Geology* **47**, 156-162. (in Chinese with English abstract).

Yang, W. Q., Liu, L., Ding, H. B., Xiao, P. X., Cao, Y. T. & Kang, L. (2012). Geochemistry, geochronology and zircon Hf isotopes of the Dimunalike granite in South Altyn Tagn and its geological significance. *Acta Petrologica Sinica*, **28**(12), 4139-4150.

Zhang, A. D. (2006). Geochemistry and geochronology of eclogites from Altyn Tagh and its geological significance. Northwest University, Doctoral dissertation (in Chinese with English abstract).

Zhang, A. D., Liu, L., Sun, Y., Chen, D. L., Wang, Y. & Luo, J. H. (2004). SHRIMP U–Pb dating of zircons and its geological significance from UHP granitoid gneiss in Altyn Tagh. *Chinese Science Bulletin* **49**, 2527–2532.

Zhang, J. X., Li, H. K., Meng, F. C., Xiang, Z. Q., Yu, S. R. & Li, J. P. (2011). Polyphase tectonothermal events recorded in "metamorphic basement" from the Altyn Tagh, the southeastern margin of Tarim Basin, Western China: constraint from U–Pb zircon geochronology. *Acta Petrologica Sinica* **27**, 23–46 (in Chinese with English abstract).

Zhang, J. X., Mattinson, C. G., Meng, F. C. & Wan, Y. S. (2005b). An early Paleozoic HP/HT granulite-garnet peridotite association in the south Altyn Tagh, NW China. P–T history and U-Pb geochronology. *Journal of Metamorphic Geology* **23**, 491–510.

Zhang, J. X., Mattinson, C. G., Yu, S. Y. & Li, Y. S. (2014). Combined rutile–zircon thermometry and U–Pb geochronology: New constraints on Early Paleozoic HP/UHT granulite in the south Altyn Tagh, north Tibet, China. *Lithos* **200**, 241-257.

Zhang, J. X., Zhang, Z. M., Xu, Z. Q., Yang, J. S. & Cui, J. W. (1999). The age of U-Pb and Sm-Nd for eclogite from the western segment of Altyn Tagh tectonic belt. *Chinese Science Bulletin* **44**, 2256–2259.

Zhang, J., Zhang, Z., Xu, Z., Yang, J. & Cui, J. (2000). Discovery of khondalite series from the western segment of Altyn Tagh and their petrological and geochronological studies. Science in China Series D: Earth Sciences, 43(3), 308-316.

Zhang, R., Zeng, Z., Zhu, Z, Chen, N., Zhao, J., Li, Q., Wang, Q. & Rao, J. (2016). LA-ICP-MS Zircon U-Pb geochorology, geochemical features and their geological implications of Paxialayidang plutons on the southern margin of Altyn Tagh. *Geological review* **62**, 1283-1299.

Zhu, X. H., Cao, Y.T., Liu, L., Wang, C. & Chen, D. L. (2014). P-T path and geochronology of high pressure granitic granulite from Danshuiquan area in Altyn Tagh. *Acta Petrologica Sinica* **30**(12) : 3717-3728